

Honeycomb structures in magnetic fields

Simon Becker,^{1,*} Rui Han,^{2,†} Svetlana Jitomirskaya,^{3,‡} and Maciej Zworski^{4,§}

¹*Department of Applied Mathematics and Theoretical Physics,*

University of Cambridge, Wilberforce Road, Cambridge, CB3 0WA, United Kingdom.

²*School of Mathematics, Georgia Institute of Technology, Atlanta, Georgia 30318, USA.*

³*Department of Mathematics, University of California, Irvine, CA 92697, USA.*

⁴*Department of Mathematics, University of California, Berkeley, CA 94720, USA.*

We consider reduced-dimensionality models of honeycomb lattices in magnetic fields and report results about the spectrum, the density of states, self-similarity, and metal/insulator transitions under disorder. We perform a spectral analysis by which we discover a fractal Cantor spectrum for irrational magnetic flux through a honeycomb, prove the existence of zero energy Dirac cones for each rational flux, obtain an explicit expansion of the density of states near the conical points, and show the existence of mobility edges under Anderson-type disorder. Our results give a precise description of de Haas-van Alphen and Quantum Hall effects, and provide quantitative estimates on transport properties. In particular, our findings explain experimentally observed asymmetry phenomena by going beyond the perfect cone approximation.

Reduced-dimensionality models are of central importance in condensed matter physics as they are often analytically solvable and allow for a qualitative description of material properties.

A phenomenologically rich class is composed of tight-binding and infinite-contrast models on periodic lattices with constant magnetic fields. Following a thorough study of these models over the past forty years, rigorous results on the fractal spectrum on the \mathbb{Z}^2 -lattice (*Harper's model*) [1]–[13], the location of the low-lying spectrum [14–17], and the disordered model (*Anderson model*) [18–20] have been obtained.

The purpose of this letter is to report rigorous results on tight-binding and infinite-contrast models for honeycomb structures in constant magnetic fields and emphasize new theoretical approaches. We consider the Hamiltonian, H^B , with constant magnetic field B , defined on edges e of a honeycomb graph Λ by

$$H_e^B := (-i\partial_x - A_e)^2 + V_e, \quad e \simeq (0, 1). \quad (1)$$

We assume Kirchhoff boundary conditions [21] at the vertices and that V_e is symmetric with respect to the centre of the edge e . Such Hamiltonians are called *quantum graphs* or *wave guides* [21, 22] and represent the infinite-contrast limits [23] of continuous Schrödinger operators on \mathbb{R}^2 with honeycomb lattice potential [24–27]. Apart from the interest in such models as limits (see [28, 29] for related work on Harper's model), quantum graphs are natural models for *molecular graphene* [30, 31] and *wave guides* [32], see Fig.3. In this letter, we explain three key physical phenomena:

- *Spectral theoretic*: We provide a full spectral analysis. In particular, we show that for irrational magnetic flux through a single honeycomb, the spectrum is a Cantor set of measure zero and Hausdorff dimension at most $1/2$ [33, 34].
- *Semiclassical*: We derive a semiclassical expansion

for the density of states (DOS) supported on geometric Landau levels and relate it to the Shubnikov-de Haas, de Haas-van Alphen, and Quantum Hall effects [35, 37]. We note a remarkable agreement of the asymptotic result with exact spectral calculations, see Fig.5. This analysis holds near each conical singularity, which we show to exist for each rational flux, thus providing a foundation for self-similarity appearing in Fig.6.

- *Dynamical*: For Anderson-type potentials in weak magnetic fields under weak disorder, we identify insulating regions away from the Landau levels in which Anderson localization occurs, and regions of metallic transport close to the Landau levels [37].

For vector potentials $A(x) = A_1(x)dx_1 + A_2(x)dx_2$ the scalar potential A_e in (1) along edges e is $A_e(x) := A(x)(e_1\partial_1 + e_2\partial_2)$ [22]. The magnetic flux $h := \int_{\odot} dA$ through each honeycomb \odot of the lattice is taken to be constant. The Hamiltonian H^B on the graph can be identified with the standard tight-binding operator t^h on the honeycomb lattice: After a simple change of geometry, the tight-binding operator t^h is

$$t^h = \frac{1}{3} \begin{pmatrix} 0 & 1 + \tau^0 + \tau^1 \\ (1 + \tau^0 + \tau^1)^* & 0 \end{pmatrix} \text{ on } \mathbb{Z}^2 \quad (2)$$

with the magnetic translations $\tau^0(r)(\gamma) := r(\gamma_1 - 1, \gamma_2)$, $\tau^1(r)(\gamma) := e^{ih\gamma_1}r(\gamma_1, \gamma_2 - 1)$ for $\gamma \in \mathbb{Z}^2$, and $r \in \ell^2(\mathbb{Z}^2; \mathbb{C})$. Solving $-y_\lambda''(x) + V_e y_\lambda(x) = \lambda y_\lambda(x)$, $y_\lambda(0) = 1, y_\lambda'(0) = 0$, we put $\Delta(\lambda) := y_\lambda(1)$. Then $\lambda \in \text{Spec}(H^B) \setminus \text{Spec}(H^D)$ (H^D is the operator (1) on a single edge with Dirichlet boundary conditions) if and only if $\Delta(\lambda) \in \text{Spec}(t^h)$ – see [29, 33, 38–40]. Since $\|t^h\| < 1$ [29, 33] for non-trivial magnetic flux $h \notin 2\pi\mathbb{Z}$ the spectrum of H^B decomposes into the disjoint union of continuous spectrum $\Delta^{-1}(\text{Spec}(t^h))$ and infinitely degenerate eigenvalues $\lambda \in \text{Spec}(H^D)$, see [33].

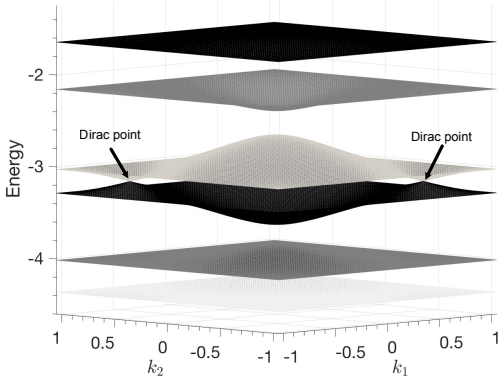


FIG. 1: We show that Dirac points persist under rational flux $\frac{h}{2\pi} \in \mathbb{Q}$. Here, $\frac{h}{2\pi} = \frac{1}{3}$ with Mathieu potential $V(x) = 20 \cos(2\pi x)$.

Cantor spectrum: The fractal structure of magnetic electron spectra was first predicted by Azbel [41] and then numerically confirmed by Hofstadter [42] for Harper's model, see Fig. 2. Verifying this experimentally is difficult as the smallness of the cell requires extraordinarily strong magnetic fields to obtain observable magnetic flux. Only recently, self-similar structures in the electron spectrum of graphene have been observed [43–46]. Earlier experiments involved modeling of periodic structures by microwaves [47]. Here, we first assume that the normalized magnetic flux $\frac{h}{2\pi} = \frac{p}{q}$ is rational, as then the Floquet-Bloch theory implies that the spectrum of (2) has band structure, see Fig. 1. We can then express the spectrum of (2) using a 1D-Jacobi operator with quasi-momentum $k \in \mathbb{T}_1^* = [0, 2\pi]$

$$(Ju)_m = \left(1 + e^{i(k+mh)}\right) u_{m+1} + 2 \cos(k + mh) u_m + \left(1 + e^{i(k+(m-1)h)}\right) u_{m-1} \quad (3)$$

and from the study of such singular Jacobi operators [33, Lemma 4.3] we estimate the Lebesgue measure

$$|\text{Spec}(t^h)| \lesssim q^{-1/2}. \quad (4)$$

The spectrum of (2) is continuous (in Hausdorff distance d_H) with respect to the magnetic flux [33, Lemma 6.2]

$$d_H(\text{Spec}(t^h), \text{Spec}(t^{h'})) \lesssim |h - h'|^{1/4}. \quad (5)$$

However, the spectral nature for irrational fluxes changes dramatically, see [33, Thm. 3]. If $\frac{h}{2\pi}$ is irrational, the spectrum of (2), and the continuous spectrum of (1), is a fully disconnected and nowhere dense set without isolated points of measure zero with Hausdorff dimension at most $\frac{1}{2}$ [34, Thm.1.5]. For irrational fluxes $\frac{h}{2\pi}$ with unbounded continued fraction expansion, the Lebesgue measure of the spectrum vanishes by combining estimate

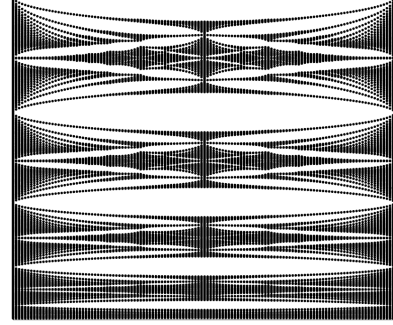


FIG. 2: Hofstadter butterfly on honeycomb lattice. The spectrum of H^B is plotted as a function of the magnetic flux $h \in [0, 2\pi]$.

(4) and the continuity estimate (5). Since the spectrum is always closed and, as can be shown, it has no isolated points, this implies Cantor-type spectrum. Using Kotani's theory, the Cantor structure of the spectrum can also be shown to hold for all irrational fluxes $\frac{h}{2\pi}$. The bound on the Hausdorff dimensions follows from an almost Lipschitz continuity estimate on the spectrum of singular quasiperiodic Jacobi operators obtained in [34].

Semiclassical analysis of the DOS: The density of states is a *generalized function* ρ_{H^B} defined in terms of the regularized trace

$$\tilde{\text{tr}}(f(H^B)) = \lim_{r \rightarrow \infty} \frac{\text{tr} \mathbf{1}_{B_r(0)} f(H^B)}{|B_r(0)|} = \int_{\mathbb{R}} f(x) \rho_{H^B}(x) dx$$

where $B_r(0)$ is the ball of radius r , see Figs. 3 and 4. By spectral equivalence of (1) and (2), for energies close to the Dirac point energy it suffices to analyze the DOS of t^h . The magnetic translations in (2) satisfy the Weyl commutation relations $\tau^1 \tau^0 = e^{ih} \tau^1 \tau^2$ and the same commutation relation is obtained for $D_x := -i \frac{\partial}{\partial x}$ by $e^{ihD_x} e^{ix} = e^{ih} e^{ix} e^{ihD_x}$ where $e^{ihD_x} = \text{Op}_h^w(e^{i\xi})$ is the Weyl quantization of the symbol $e^{i\xi}$ [48]. This different representation reduces the analysis of the DOS of (2) to the study of the DOS of the operator

$$\frac{1}{3} \begin{pmatrix} 0 & 1 + e^{ix} + \text{Op}_h^w(e^{i\xi}) \\ 1 + e^{-ix} + \text{Op}_h^w(e^{-i\xi}) & 0 \end{pmatrix}. \quad (6)$$

Through a symplectic change of variables, $y = a(x + \xi)$, $\eta = b(\xi - x \pm \frac{4\pi}{3})$, ($a = \pm 2^{-\frac{1}{2}} 3^{-\frac{1}{4}}$, $b = \pm 2^{-\frac{1}{2}} 3^{\frac{1}{4}}$) one finds that at the Dirac points we have

$$\begin{aligned} 1 + e^{ix} + e^{i\xi} &= c(\eta \mp iy) + \mathcal{O}(y^2 + \eta^2), \\ 1 + e^{-ix} + e^{-i\xi} &= c(\eta \pm iy) + \mathcal{O}(y^2 + \eta^2), \end{aligned} \quad (7)$$

$c = 3^{\frac{1}{4}} 2^{-\frac{1}{2}}$. Classical-quantum correspondence implies that by the symplectic change of variables (*classical*),

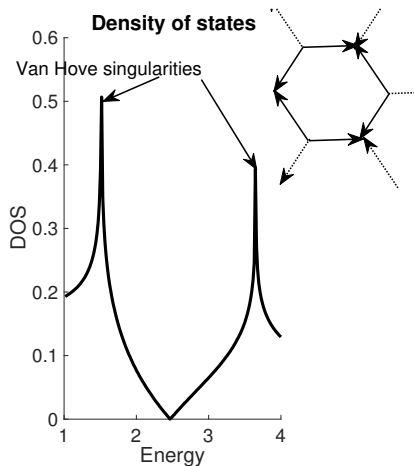


FIG. 3: The DOS of the quantum graph model without magnetic field obtained using $H^{B=0}$ (1) and $V = 0$ on the first band $[0, \pi^2]$. The comparison with [30] Fig.1 shows a good agreement of the model with molecular graphene experiments.

operator (6) is (micro)-locally equivalent (*quantum*) to the operator $\frac{c}{3} \begin{pmatrix} 0 & a_{\pm}^* \\ a_{\pm} & 0 \end{pmatrix}$ quantized in new variables $a_{\pm} := y \pm ihD_y$. The spectrum of this operator can be explicitly expressed through the quantum harmonic oscillator. By making these steps precise and taking higher order contributions of the geometry in (7) into account, it is possible to show the semiclassical Bohr-Sommerfeld description of the DOS with precise error control [35, Thm. 1]: If $I \subset \Delta^{-1}(-\delta, \delta)$, with $\delta > 0$ small, then

$$\begin{aligned} \tilde{\text{tr}}f(H^B) &= \frac{2h}{3\sqrt{3}\pi} \sum_{n \in \mathbb{Z}^2} f(z_n(h)) + \mathcal{O}(|f|_{C^\alpha} h^\infty) \\ \Delta(z_n(h)) &= \kappa(nh, h), \quad \alpha > 0, \end{aligned} \quad (8)$$

$\kappa(nh, h)$ are the solutions to the Bohr-Sommerfeld condition $F(\kappa(\zeta, h)^2, h) = |\zeta| + \mathcal{O}(h^\infty)$ with the expansion

$$\begin{aligned} F(s, h) &\sim F_0(s) + \sum_{j=2}^{\infty} h^j F_j(s), \quad F_0(s) = \frac{1}{4\pi} \int_{\gamma_s} \xi dx, \\ \gamma_s &= \left\{ (x, \xi) \in \mathbb{T}_*^2 : \frac{|1 + e^{ix} + e^{i\xi}|^2}{9} = s \right\}, \quad F_j(0) = 0. \end{aligned} \quad (9)$$

In particular, we show that $F_1(s) = 0$ for all such 2×2 operators with only off-diagonal contributions. Writing $g(x) = F_0(\Delta(x)^2)$, we obtain a leading order approximation of Landau levels

$$z_{\pm|n|}^{(1)}(h) = g_{\pm}^{-1}(|n|h), \quad z_0^{(1)}(h) = 0. \quad (10)$$

In (8), $|f|_{C^\alpha} := \sup_x |f(x)| + \sup_{x \neq y} \frac{|f(x) - f(y)|}{|x - y|^\alpha}$: it is essential to allow non-smooth test functions f in view of applications to magnetic oscillations. (See for instance [36] for a physics perspective on semiclassical approximation in this setting.)

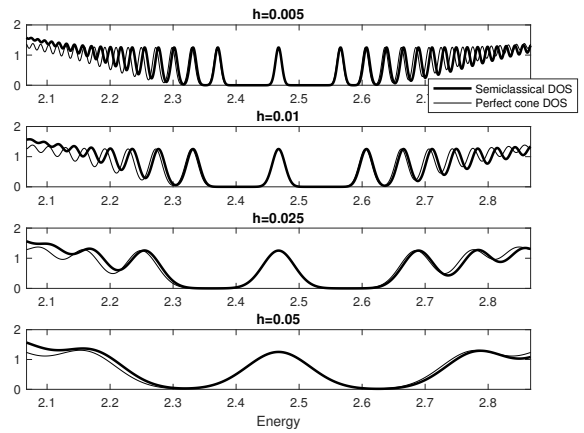


FIG. 4: *Shubnikov-de Haas oscillations* of $\mu \mapsto \rho_{HB}(\exp((\bullet - \mu)^2/2\sigma^2)/\sqrt{2\pi}\sigma)$ for different values of h . We note the asymmetry when compared to the DOS assuming perfect cones.

Fig.4 shows that Landau levels, and thus the DOS are non-symmetric with respect to the Dirac point energy. We compare this with the symmetric leading order (*perfect cone*) approximation of phase space area $g_c(x) = (x - z_D)^2/v_F^2$ with Fermi velocity $v_F = 3^{-3/4}\Delta'(z_D)^{-1}$ and Dirac point energy $z_D \in \Delta^{-1}(0)$. (8) also explains *de-Haas van Alphen oscillations*. To formulate it we introduce the *grand-canonical potential* with inverse temperature β and chemical potential μ :

$$\begin{aligned} \Omega_\beta(\mu, h) &:= \rho_B(\eta(\bullet)f_\beta(\mu - \bullet)), \\ f_\beta(x) &:= -\beta^{-1} \log(e^{\beta x} + 1) \simeq -x_+, \quad \beta \rightarrow +\infty, \end{aligned} \quad (11)$$

for smooth η localizing to energy intervals contained in $\Delta^{-1}(-\delta, \delta)$. (Note that $|f_\beta|_\alpha$ is uniformly bounded for $\alpha \leq 1$ but not for $\alpha > 1$.) The *magnetization* is defined by [49]

$$M_\beta(\mu, h) := -\frac{3\sqrt{3}}{2} \frac{\partial}{\partial h} \Omega_\beta(\mu, h). \quad (12)$$

and at zero temperature, we can derive from this a *sawtooth approximation*, with $\sigma(y) := y - [y] - \frac{1}{2}$, as the $\mathcal{O}(h^{\frac{1}{2}})$ approximation of (12) given as

$$M_\infty(\mu, h) = \frac{1}{\pi} \sigma \left(\frac{g(\mu)}{h} \right) \frac{g(\mu)}{g'(\mu)} + \mathcal{O}(h^{\frac{1}{2}}). \quad (13)$$

This provides a refinement of results found in [50–52]. The remarkable agreement of the different expressions for the magnetization is illustrated in Fig.5: the characteristic sawtooth pattern (13) is compared with the magnetization computed from (12), using either the operator spectrum or the semiclassical limit (8).

QHE and self-similarity: One of the striking properties of graphene is the presence of Dirac points, which has remarkable physical and technological implications [53].

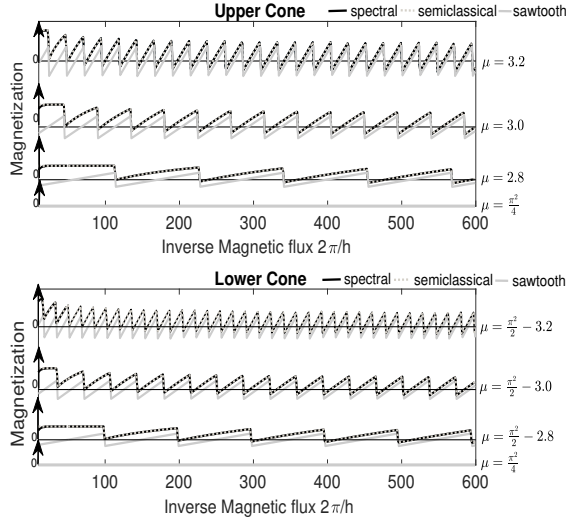


FIG. 5: Magnetization for different chemical potentials above/below the Dirac energy $\mu = \frac{\pi^2}{4}$, with $V \equiv 0$.

It turns out Dirac points are present at $E = 0$ for any magnetic flux $h = 2\pi p/q$, [37, Thm. 2]. To study transport properties on honeycomb structure (see [54–57]) we consider operator (2) with additive disorder

$$t_{\kappa,\omega}^h = \frac{1}{3} \begin{pmatrix} -\kappa V_{\omega}^{(1)} & 1 + \tau^0 + \tau^1 \\ (1 + \tau^0 + \tau^1)^* & -\kappa V_{\omega}^{(2)} \end{pmatrix}, \quad (14)$$

where $(V_{\omega}^{1,2})_{z \in \mathbb{Z}^2}$ are i.i.d. random variables with compactly supported probability distribution and small $\kappa > 0$. For discrete operators A with \mathbb{C}^2 -valued kernel $(A(x, y))$, we define a regularized trace

$$\widehat{\text{tr}} A := \lim_{r \rightarrow \infty} \frac{1}{|B_r(0)|} \sum_{\gamma \in \Lambda \cap B_r(0)} \text{tr}_{\mathbb{C}^2} A(\gamma, \gamma). \quad (15)$$

$$\widehat{\text{tr}} f(t^B) = \frac{2q\varepsilon}{3\sqrt{3}\pi} \sum_{n \in \mathbb{Z}^2} f(z_n(h)) + \mathcal{O}(|f|_{C^\alpha} \varepsilon^\infty)$$

where $z_n(\varepsilon) = v_F \text{sgn}(n) \sqrt{|n\varepsilon|} + \mathcal{O}(\varepsilon)$ and

$$v_F = 3^{3/4} q \left(3^{q-1} \prod_{j=q+2}^{2q} t_j^{B_0}(\tilde{k}) \right)^{-1}. \quad (16)$$

Here, $t_j^{B_0}(\tilde{k})$ is the j -th Floquet eigenvalue to t^{B_0} with quasimomentum \tilde{k} where B_0 is the magnetic field associated to the flux $h_0 = \frac{2\pi p}{q}$. This study is inherently connected with self-similarity in the Hofstadter butterfly, see Fig.6, and the occurrence of magnetic mini-bands [44]. Since t^B is an element of the rotation algebra, so is its Fermi projection $P = \mathbb{1}_{[z_D, \mu]}(t^B)$ for Fermi energies μ inside a spectral gap of t^B . By [58–60], there is $\gamma \in \mathbb{Z}^2$, such that

$$\widehat{\text{tr}}(P) = \frac{2}{3\sqrt{3}} (\gamma_1 + \gamma_2 \frac{\varepsilon}{2\pi}) \quad (17)$$

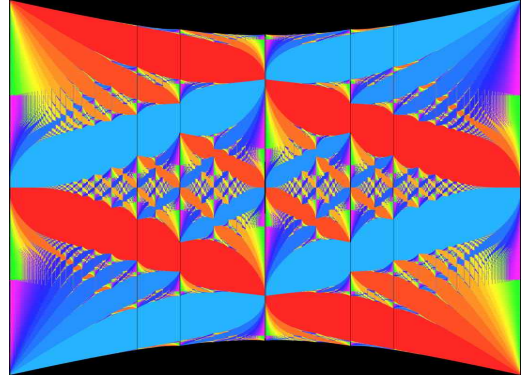


FIG. 6: Hofstadter butterfly on honeycomb lattice. Different colours correspond to different Hall conductivities.

where by (16) we see that $\gamma = (0, 2qn)$ and n is the number of Landau levels between z_D and μ . Combining (16) with (4) implies the existence of spectral gaps between a finite number of disjoint intervals $\mathcal{B}_n(h) \ni z_n(h)$ up to some small disorder strength $\kappa_0 > 0$. The Hall conductivity, which by universality (see [61, 62]) is invariant under weak disorder, is given by Středa's formula [63] as $c_H(\mu) := \frac{\partial}{\partial h} \widehat{\text{tr}}(\mathbb{1}_{[z_D, \mu]}(t_{\kappa,\omega}^h)) = \frac{\gamma_2}{2\pi}$ with Fermi energies μ in the interval I_n between $B_n(h)$ and $B_{n+1}(h)$ [37, Prop.1.1 & Thm. 4]. From (16) and (17) we then find

$$c_H(\mu) = \begin{cases} \frac{(2n+1)q}{2\pi}, & \mu \in I_n, n \geq 0 \\ \frac{(2n-1)q}{2\pi}, & \mu \in I_{n-1}, n \leq 0. \end{cases} \quad (18)$$

This expression is only valid for Fermi energies close to the conical point. The Hall conductivity for arbitrary Fermi energies is far more intricate, see Fig.6, [54, 64].

Metal/insulator transition: The Hall conductivity allows us also to analyze transport properties of $t_{\kappa,\omega}^h$. Transport in disordered media at energy E is measured by transport coefficients $\beta_{\kappa}^h(E)$ [20, 65–68]. This quantity allows us to define two complementary energy regions, the *insulator region* $\Sigma_{\kappa}^{h,DL} = \{E \in \mathbb{R}; \beta_{\kappa}^h(E) = 0\}$ and the *metallic transport region* $\Sigma_{\kappa}^{h,DD} = \{E \in \mathbb{R}; \beta_{\kappa}^h(E) > 0\}$. Energies $E \in \Sigma_{\kappa}^{h,DD}$ at which the transport coefficient β_{κ}^h jumps from zero to a non-zero value are called *mobility edges*, while energies $E \in \Sigma_{\kappa}^{h,DL}(H_{\kappa,\omega}^h)$, that also belong to the spectrum of (14), are eigenvalues of finite multiplicity with exponentially decaying eigenfunctions (*Anderson localization*). From the jumps of the Hall conductivity, we conclude [37, Thm. 1] that there exist mobility edges E close to each Landau level with non-trivial transport $\beta_{\lambda}^h(E) \geq 1/4$. In contrast to this, we show by verifying the starting criteria of the multi-scale analysis [19, 37, 66] that the spectral gaps between the Landau levels can only be filled with spectrum belonging to the insulating region [37, Prop.5.5] in which the operator (14) therefore exhibits Anderson localization.

Acknowledgements. S.B. gratefully acknowledges support by the UK Engineering and Physical Sciences Research Council (EPSRC) grant EP/L016516/1 for the University of Cambridge Centre for Doctoral Training, the Cambridge Centre for Analysis. R.H., S.J., and M.Z. were partially supported by the National Science Foundation under the grants DMS-1800689, 1500852 and 1901462.

* simon.becker@damtp.cam.ac.uk

† rui.han@math.gatech.edu

‡ szhitomi@math.uci.edu

§ zworski@math.berkeley.edu

- [1] J. Bellissard, B. Simon, J. Func. Anal. **48** 408-419, (1982)
- [2] J. Avron, P. van Mouche, B. Simon: Comm. Math. Phys. **132**, 103–118 (1990).
- [3] Y. Last. Comm. Math. Phys. **164**, 421–432, (1994).
- [4] S. Jitomirskaya, Y. Last, Comm. Math. Phys. **195**, 1-14 (1998).
- [5] S. Jitomirskaya and I. Krasovskiy. Math. Res. Lett. **9**, 413–421 (2002).
- [6] J. Puig, Comm. Math. Phys. **244**, 297-309 (2004).
- [7] A. Avila, R. Krikorian. Ann. Math. **164**, 911-940 (2006)
- [8] A. Avila, S. Jitomirskaya, in *The Ten Martini problem*. Lect. Notes in Physics. 690. pp. 5-16, (2005)
- [9] S. Jitomirskaya and S. Zhang. *arXiv:1510.07086*, 2015.
- [10] Y. Last and M. Shamis. Comm. Math. Phys. **348**, 729–750 (2016).
- [11] A. Avila, S. Jitomirskaya and C. Marx. Inv. Math. **210.1**, 283–339 (2017)
- [12] R. Han, Tran. AMS, 370 (2018), 197-217.
- [13] B. Helffer, Q. Liu, Y. Qu, Q. Zhou. Comm. Math. Phys., **368**, 369382 (2019).
- [14] B. Helffer and J. Sjöstrand, Mém. Soc. Math. France (N.S.) **34**, (1989).
- [15] B. Helffer and J. Sjöstrand, in *Schrödinger operators (Sønderborg, 1988)*, 118–197 Lect. Not. in Phys.**345**, Springer, Berlin, (1989).
- [16] B. Helffer and J. Sjöstrand, Mém. Soc. Math. France (N.S.) **40**, (1990).
- [17] B. Helffer and J. Sjöstrand, *On diamagnetism and de Haas-van Alphen effect*. Ann. Inst. H. Poincaré Phys. Théor. **52**, 303–375, (1990).
- [18] P. W. Anderson, Phys. Rev. 109 (5): 1492-1505, (1958).
- [19] J. Fröhlich and T. Spencer, (1983).Comm. Math. Phys. Volume 88, Number 2, 151-184.
- [20] F. Germinet, A. Klein, J. Schenker,Ann. of Math., 166, 215-244, (2007).
- [21] P. Kuchment and O. Post,Comm. Math. Phys, **275(3)**, 805–82, (2007).
- [22] V. Kostykin, R. Schrader. Comm. Math. Phys. 237 (2003), 161 - 179.
- [23] B. Helffer, P. Kerdelhué, and J. Royo-Letelier. Annales Henri Poincaré, **17**, Issue 4, (2016).
- [24] C. Fefferman and M. Weinstein, J. Amer. Math. Soc. **25**, 1169–1220, (2012).
- [25] C. Fefferman, J. Lee-Thorp, M. Weinstein Comm. Pure and Appl. Math. Volume 71, Issue 6, (2016).
- [26] A. Drouot, C. Fefferman and M. Weinstein *arXiv:1810.05875*, (2018).
- [27] A. Drouot, Communications in PDEs 44(2019), no 12, 1406-1430.
- [28] A. Avila, and S. Jitomirskaya, Annals of Mathematics, 170(1), pp. 303-342, (2009).
- [29] J. Brüning, V Geyler, and K. Pankrashkin, Comm. Math. Phys., **269(1)**, 87–105, (2007).
- [30] K.K. Gomes, W. Mar, W. Ko, F. Guinea and H.C. Manoharan, Nature **483**, 306–310, (2012).
- [31] M. Polini, F. Guinea, M. Lewenstein, H.C. Manoharan and V. Pellegrini Nature Nanotechnology **8**, 625–633, (2013).
- [32] U. Kuhl and H.-J. Stöckmann, Phys. Rev. Lett., 80,15, 3232–3235, (1998).
- [33] S. Becker, R. Han, and S. Jitomirskaya, Inv. Math. 218, 979–1041 (2019).
- [34] S. Jitomirskaya and I. Krasovskiy, *arXiv:1909.04429*
- [35] S. Becker and M. Zworski, Comm. Math. Phys., Vol. 367, Issue 3, pp 941-989, (2019).
- [36] P. Carmier and D. Ullmo, Phys. Rev.B77, 245413, (2008).
- [37] S. Becker and R. Han, (2019). *arXiv:2004.06189*.
- [38] K. Pankrashkin, Letters in Math. Physics, 77(2), pp. 139-154, (2006).
- [39] K. Pankrashkin, J. Funct. Anal. 265 (2013) 2910-2936, 640-655, (2013).
- [40] K. Pankrashkin, J. Math. Anal. Appl. 396, 640-655, (2012).
- [41] M. Azbel, Sov. Phys. JETP 19.3., pp. 634-645, (1964).
- [42] D. Hofstadter,Physical Review B 14.6, pp. 2239-2249. (1976).
- [43] X. Chen, A. Wallbank, A. Patel, M. Mucha-Kruczynski, E. McCann, and V. Falko Phys. Rev. B 89.7: 075401, (2014).
- [44] X. Chen, J.. Wallbank, A.. Patel, M. Mucha-Kruczynski, E.. McCann, and V.. Fal’ko (2014), Phys. Rev. B, 89, 7. Nature 497, pp. 598-602, (2013).
- [45] H. Garcia-C., L. Gaggero-S., D.S. Díaz-G., O. Sotolongo-C., and I. Rodríguez-V.,Sc. Reports 7.1. 617, (2017).
- [46] L. Ponomarenko et al, Nature 497, pp. 594-597, (2013).
- [47] U. Kuhl and H.-J. Stöckmann, Phys. Rev. Lett., 80,15, 3232–3235, (1998).
- [48] M. Zworski, *Semiclassical Analysis*, AMS, (2012).
- [49] L. Onsager, Philos. Mag.7, 43, (1952).
- [50] S.G. Sharapov, V.P Gusynin, H.Beck, Phys. Rev. B.69, 075104, (2004).
- [51] A. Lukyanchuka, Low Temp. Phys.37, 45, (2011).
- [52] T. Champelde, VP. Mineev, VP, Philos. Mag. B81, 55-74 (2001).
- [53] H.-S. P. Wong, D. Akinwande, Cambridge University Press, 2010.
- [54] A. Agazzi, J.-P. Eckmann, G.-M. Graf,Journal of Stat. Phys., 156(3), (2014).
- [55] V. P. Gusynin and S. G. Sharapov, Phys. Rev. B 73, 245411, (2006).
- [56] N. Peres, Rev. of Mod. Phys. 82(3), (2010).
- [57] S. V. Morozov, K. S. Novoselov, M. I. Katsnelson, F. Schedin, L. A. Ponomarenko, D. Jiang, and A. K. Geim, Phys. Rev. Lett. 97, 016801, (2006).
- [58] M. Pimsner and D. Voiculescu, J. Operator Theory (4), 93-118,(1980)
- [59] M. Pimsner and D. Voiculescu, (1980) J. Operator Theory (4), 201-210.
- [60] M. A. Rieffel, Pacific J. Math., 93, 415–429 (1981).
- [61] J. Avron, R. Seiler, and B. Simon Comm. Math. Phys.,

- 159**:399–422, (1994).
- [62] J. Bellissard, A. van Elst, and H. Schulz-Baldes, (1994).
J. Math. Phys., **35**:5373–5451, (1994).
- [63] P. Středa, J. Phys. C: Solid State Phys., **15**:L717, (1982).
- [64] Y. Zhang, Y. Wen Tan, H. Stormer and P. Kim, Nature
volume 438, pages 201-204, (2005).
- [65] F. Germinet, A. Klein, Comm. Math. Phys., Volume 222,
Issue 2, pp 415-448, (2001).
- [66] F. Germinet, A. Klein, Geom. funct. anal. Vol. 13, 1201-
1238, (2003).
- [67] F. Germinet and A. Klein, Duke Math. J. Volume 124,
Number 2, 309-350, (2004).
- [68] F. Germinet and A. Klein, Journal of Stat. Phys. Vol.
122, No. 1, (2006).